Comparison between AMSR-E ASI sea-ice concentration product, MODIS and pseudo-ship observations of the Antarctic sea-ice edge

Xi ZHAO,[1] Haoyue SU,[1] Alfred STEIN,[2] Xiaoping PANG[1]

[1]*Chinese Antarctic Center of Surveying and Mapping, Wuhan University, Wuhan, China*
E-mail: pxp@whu.edu.cn
[2]*Faculty of Geo-Information Science and Earth Observation, Twente University, Twente, The Netherlands*

ABSTRACT. The performance of passive microwave sea-ice concentration products in the marginal ice zone and at the ice edge draws much attention in accuracy assessments. In this study, we generated 917 pseudo-ship observations from four Moderate Resolution Imaging Spectroradiometer (MODIS) images based on the Antarctic Sea Ice Processes and Climate (ASPeCt) protocol to assess the quality of the Advanced Microwave Scanning Radiometer for Earth Observing System (AMSR-E) ARTIST (Arctic Radiation and Turbulence Interaction STudy) Sea Ice (ASI) concentrations at the ice edge in Antarctica. The results indicate that the ASI pixels in the pseudo-ASPeCt observations have a mean ice concentration of 13% and are significantly different from the well-established 15% threshold. The average distance between the pseudo-ice edge and the 15% threshold contour is ~10 km. The correlation between the sea-ice concentration (SIC), SIC_{ASI} and SIC_{MODIS} values at the ice edge was considerably lower than the high coefficients obtained from a transect analysis. Underestimation of SIC_{ASI} occurred in summer, whereas no clear bias was observed in winter. The proposed method provides an opportunity to generate a new source of reference data in which the spatial coverage is wider and more flexible than in traditional in situ observations.

KEYWORDS: sea ice

INTRODUCTION

Sea ice is sensitive to temperature changes, and its changing extent serves as an indicator of climate change in polar regions (Massom and Stammerjohn, 2010). Therefore, accurately identifying the location of the ice edge is important for estimating the total ice extent and for determining the overall mass balance of sea-ice coverage (Parkinson and Cavalieri, 2012). From the first satellite microwave radiometers launched in 1972 until now, passive microwave radiometers have provided full coverage of the polar regions. Among them, the Advanced Microwave Scanning Radiometer for Earth Observing System (AMSR-E) has the highest spatial resolution (6.25 km) and has a wide range of frequencies that provide a more accurate measure of sea-ice extent (Spreen and others 2008).

The publicly distributed standard AMSR-E sea-ice concentration (SIC) products are generated using the ARTIST (Arctic Radiation and Turbulence Interaction STudy) Sea Ice (ASI) algorithm at 6.25 km resolution and the NASA Team 2 (NT2) algorithm at 12.5 and 25.0 km resolution. Previous studies have compared SIC retrieval with retrieval from higher-resolution optical and synthetic aperture radar (SAR) sensors (e.g. Heinrichs and others, 2006; Lee and Han, 2008), as well as with in situ ship observations (e.g. Worby and Comiso, 2004; Ozsoy-Cicek and others, 2011). These assessments were generally positive and indicated strong agreement of SIC with similar formations of the sea-ice edge among different satellite data (Heinrichs and others, 2006). Cavalieri and others (2006) assessed the performance of AMSR-E NT2 products using Landsat ETM+ and airborne microwave imagery under winter conditions in the Arctic, and found a bias ranging from 0% to 3% and a root-mean-square error (RMSE) ranging from 1% to 7% for all ice types. On the other hand, the ASI algorithm, which can offer higher-resolution

SIC estimates, was assessed by Wiebe and others (2009) using the same validation data as Cavalieri and others (2006). Averaged over all ice types, the bias ranged between 2.0% and 17.4%, and new ice had a lower accuracy than first-year and young ice. For the more complex Antarctic winter sea ice, Cavalieri and others (2010) compared AMSR-E NT2 products with ten Moderate Resolution Imaging Spectroradiometer (MODIS) images and observed that the averaged SIC biases relative to MODIS ranged from <–0.5% to –18%, and the RMSE ranged from 2% to 24%. These values were much higher than in the Arctic. Furthermore, the bias and RMSE were correlated with the fractions of new ice and open water, indicating that the largest errors occurred in the marginal ice zone and along the ice edge. Other previous research also pointed to a relatively low agreement in the marginal edge zone, especially during the ice melt season (e.g. Worby and Comiso, 2004; Ozsoy-Cicek and others, 2009, 2011; Wiebe and others, 2009). This study mainly focused on areas with potentially lower accuracy; therefore, the focus was on the assessment of the sea-ice edge in the Antarctic during summer.

An ice concentration threshold of 15% is commonly used when determining the sea-ice edge from passive microwave ice concentration products. Worby and Comiso (2004) questioned the reliability of sea-ice edge derived from 15% SIC. After comparing edge locations observed by Special Sensor Microwave/Imager (SSM/I), ships and a variety of optical and SAR images, they found that 1–2° latitude (>100 km) offsets occurred in the summer ice-edge locations. Heinrichs and others (2006) assessed the AMSR-E ice concentration product at the ice edge and arrived at the more inspiring conclusion that the position of the ice edge determined by 15% SIC was on average within one AMSR-E grid square (12.5 km) of the ice edge determined from SAR

data. Similarly, Ozsoy-Cicek and others (2009) validated the AMSR-E NT2 product using ship observations from the *Oden* expedition during an Antarctic summer. They determined that the AMSR-E-derived ice edge was further south and that there was a poor correlation between ship observations and the AMSR-E SIC. All the ship observations mentioned above were recorded using a standard protocol from the Antarctic Sea Ice Processes and Climate (ASPeCt) program within the Scientific Committee on Antarctic Research (Worby and Allison 1999).

Although ship observation records obtained from Antarctic expeditions have been used to map the sea-ice edge and have been compared with satellite-derived data, the number of ship observations that are located exactly at the sea-ice edge is very limited. For example, there are 36 ice-edge data points presented in Worby and Comiso (2004); of a total of 384 ship observations during two ship cruises, 58 were in the marginal zone (Ozsoy-Cicek and others, 2011). However, to assess the ice-edge accuracy by performing reliable statistical analysis, a sufficient number of observations at the ice edge are required. In this context, we propose a new method to generate pseudo-ship observations from optical satellite images, in accordance with the ASPeCt standard ship-based observation protocol. The number of ice-edge data points was expected to be greatly expanded with this method. Furthermore, the spatial coverage of the pseudo-ship observations would be wider and more flexible than in situ observations, which are constrained by the cruise route.

METHODOLOGY

This study used data from an AMSR-E ASI dataset and a MODIS dataset. The MODIS data were classified to sea-ice binary maps, and pseudo-ship observations were then generated based on ASPeCt. The datasets are described and the method of processing is explained below.

Dataset I: AMSR-E ASI ice concentration (SIC_{ASI})

The AMSR-E sensor was operating aboard the NASA Aqua platform between 2002 and 2011. It provides data on both horizontally and vertically polarized brightness temperatures at six different frequencies between 6.9 and 89.0 GHz. Standard AMSR-E daily sea-ice concentrations are derived using the NASA NT2 algorithm (Markus and Cavalieri, 2000), with spatial resolutions of 12.5 and 25.0 km. The ASI algorithm (Kaleschke and others, 2001; Spreen and others, 2008) was developed as a way to obtain more detail from the high spatial resolution of the 89 GHz channels and shows a performance similar to other sea-ice algorithms (Spreen and others, 2008). In this study, we selected an ASI ice concentration grid at a 6.25 km spatial resolution to capture the edge location. Because the ASI is applied to daily average products and not to daily ascending or descending images, a publicly distributed ASI daily average grid was chosen to enable users of the products to benefit from a better understanding of their qualities.

Daily average ASI grids (SIC_{ASI}) with a 6.25 km resolution were obtained using the current version of the ASI algorithm, which is described in detail by Spreen and others (2008). All the data were produced by the Institute of Environmental Physics (IUP) at the University of Bremen, Germany, and were downloaded from http://iup.physik.uni-bremen.de:8084/amsredata/asi_daygrid_swath/l1a/s6250/. The SIC_{ASI}

were in a GeoTIFF format, which is available as bytes (0–255) and with a polar stereographic projection. The ice concentrations between 0% and 100% were scaled to values between 0 and 200, so that every value of the GeoTIFF byte data represents a 0.5% ice concentration range.

Dataset II: MODIS

The MODIS image was chosen to serve as the primary independent evaluation source. MODIS has 36 visible/infrared bands with spatial resolution ranging from 250 m to 1 km. Four MODIS images were obtained for the dates when the synchronous Landsat TM images also had atmospherically clear conditions. Although MODIS has a coarser resolution than TM, it covers a much wider swath, thereby permitting greater coverage of both AMSR-E pixels and ice edges. Landsat TM images were used in this study as a secondary referencing source for explaining our results.

The four MODIS scenes that were used in this study cover portions of the Weddell Sea, Pacific Ocean and Bellingshausen Sea (Fig. 1). The MOD 02–Level-1B Calibrated Geolocation Data Set were downloaded from the Atmosphere Archive and Distribution System (http://ladsweb.nascom.nasa.gov). Using a MODIS geolocation product, a sun-angle correction was applied to the reflectance of band 1 (0.620–0.670 m) and band 2 (0.841–0.876 m) at a 250 m resolution and to band 4 (0.545–0.565 m) and band 6 (1.628–1.652 m) at a 500 m resolution, to generate top-of-the-atmosphere reflectance. Next the top-of-the-atmosphere reflectances for each band in swath form were transformed into a polar stereographic projection.

Data processing I: sea-ice binary map and pseudo-ASPeCt observations

A multiple thresholds method was employed following NASA's MODIS sea-ice product processing approach (Riggs and others, 2006). This approach defines ice and no-ice thresholds using multiple bands, by allowing each MODIS pixel to be classified either as ice or not ice. First we regridded bands 4 and 6 to a 250 m resolution and calculated the normalized-difference snow index (NDSI) using $NDSI = (Ref_{band4} - Ref_{band6})/(Ref_{band4} + Ref_{band6})$, where Ref_{band4} and Ref_{band6} indicate the reflectance of bands 4 and 6, respectively. Next if a MODIS pixel fulfilled the three criteria $NDSI > 0.4$, $Ref_{band1} > 0.1$ and $Ref_{band2} > 0.11$, it was labeled as ice, otherwise it was labeled as no ice. Using this method, the MODIS images were classified into binary sea-ice maps with values of 1 (ice) and 0 (no ice) at a 250 m resolution. This binary map was used to generate pseudo-ship points in the next step.

The sea-ice edge was defined as the northernmost occurrence of sea ice with at least a 10% concentration, where the ice concentration within a 1 km radius of the ship is estimated from the ship's bridge (Worby and Comiso, 2004). To simulate the ice-edge determination it was necessary to 'look at' an ice concentration map from space with a 1 km radius, instead of from a ship, and to identify the northernmost 10% concentration point. In this study we replaced the 1 km radius with a 2 km resolution grid, which was derived from the binary ice map by averaging the values of every 8×8 cell grid. Next, we established the contours of a 10% SIC from the 2 km ice concentration grid and marked the ASI pixels passing the contours as pseudo-ship-observed pixels. In total, 917 pseudo-ASPeCt observations were sampled from four scenes (Table 1).
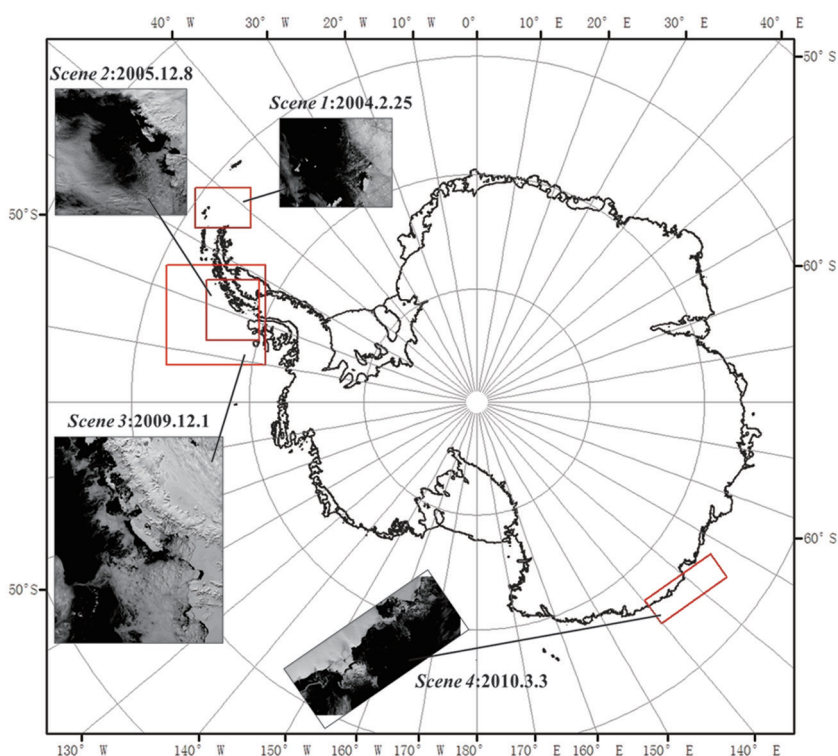
Fig. 1. Location of the four MODIS scenes in the Antarctic. Date format is year.month.day.

Data processing II: comparison of ice edges and transects

Ideally, we might expect that all 917 ASI pixels covering pseudo-ASPeCt observations have the same SIC value of 15%; if so, the 15% threshold for passive microwave images would be pertinent. To be more flexible, we hypothesized that the mean concentration should not be significantly different from 15%. Furthermore, the 917 ASI pixels should have concentration values (SIC_{ASI}) similar to their corresponding MODIS pixels (SIC_{MODIS}). SIC_{MODIS} is calculated as the average value of the 25×25 cells on a binary ice map that match the size of the corresponding 6.25 km ASI pixel. Descriptive statistics and a correlation analysis were performed to compare SIC_{ASI} and SIC_{MODIS} data. In addition to the ice concentrations, the spatial variability of the ice edges was also considered. The outlines of the cell regions with a 10% concentration on the 2 km resolution grid were marked as the pseudo-ice edge. The distance between the

location of the pseudo-ice edge and the 15% SIC_{ASI} contour was analyzed.

To assess the accuracy of SIC_{ASI} at the ice edge with that in open water and in the interior zone, we drew eight transects (i.e. two on each scene). All the transects started at the ice interior, passed the ice edge and marginal zone, and reached the open water. The SIC_{ASI} and SIC_{MODIS} data along these transects were compared. The pseudo-ASPeCt observations on the transects were marked out to be compared with the 15% SIC.

RESULTS

Comparison of ASI ice concentration (SIC_{ASI}) and pseudo-ASPeCt observations

The summary statistics of SIC_{ASI} at the pseudo-ASPeCt points for each scene are shown in Table 1. The mean and standard deviation of SIC_{ASI} ranged from 0.8% to 19.9% and 2.9% to

Table 1. Details of the four MODIS scenes and a comparison of SIC_{ASI} and SIC_{MODIS} from pseudo-ASPeCt observations

	Date	Number of edge points	SIC_{ASI}		Z test for difference with 15%	$SIC_{ASI} - SIC_{MODIS}$		
			Mean	Std dev.		Bias	RMS	R^2
			%	%		%	%	
Scene 1	25 Feb 2004	98	0.8	2.9	−48.376*	−15.1	19.2	0.2*
Scene 2	8 Dec 2005	364	10.6	21.4	−3.051*	−12.3	30.5	0.03*
Scene 3	1 Dec 2009	182	12	17.9	−2.301*	−12.8	28	0.1*
Scene 4	3 Mar 2010	273	19.9	24.1	13.648*	0.5	26.2	0.05*
Total		917	13	21.2	−2.903*	−8.9	27.7	0.04*

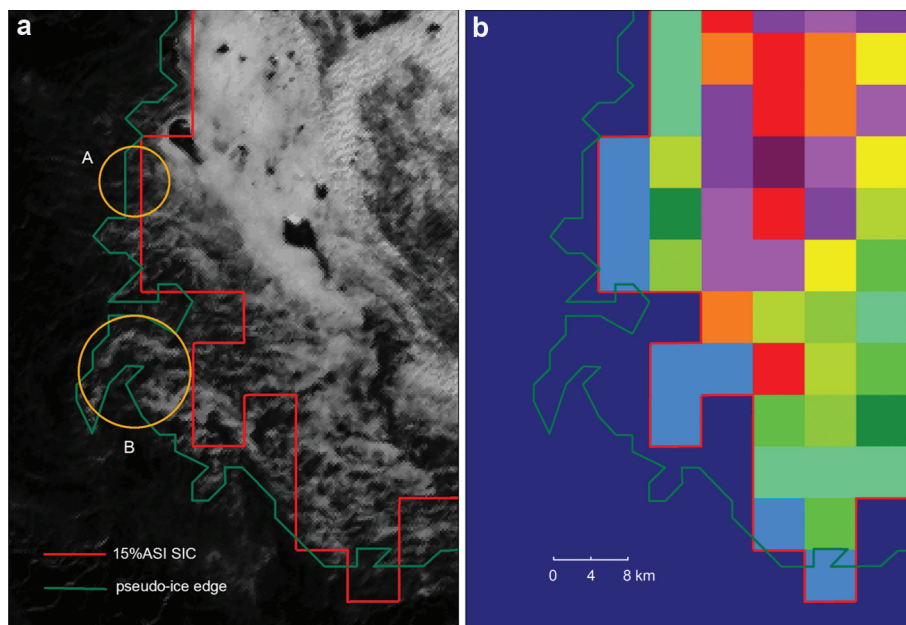*Statistically significant at a 0.05 level.

Fig. 2. Contour of the 15% ASI SIC threshold and the pseudo-ice edge overlaid on the original MODIS band 2 (a) and the ASI concentration product (b). This region is the subset of scene 2. Yellow circles highlight regions A and B where representative types of gaps occur.

24.1%, respectively. Scenes 2, 3 and 4 had similar mean ice concentrations of ∼15% and standard deviations of ∼20%. The closest concentration to the 15% standard threshold was 12%, derived from scene 3. Of the four scenes, scene 1 is the exception, with a lower mean concentration and smaller standard deviation than the others. Putting all the sample points together, we observed that the mean SIC_{ASI} value was 13%. Means testing (Z tests) indicated that all the mean values were significantly different from 15% at a 0.05 significance level, although a 2% difference seems remarkably good. The reason could be the large number of sample points. Therefore, the difference between the mean and 15% was so large that we know with 95% certainty the difference was not by chance.

Although the differences between the ice concentration values were significant, the spatial separation of the edges could be small. For example, the ice edges derived from the ASI and ASPeCt observations have a small distance within one or half a pixel size, but their concentration values can be significantly different. Consequently, we checked the spatial locations of the 15% ASI threshold and pseudo-ice edges, and overlaid these on the original MODIS image and the ASI product (similar to Fig. 2). Generally, the 15% ASI contour was located south of the pseudo-ice edge. We found that the average distance between the two lines did not exceed three ASI pixels, whereas 58% of the separation space is approximately one pixel in width. Some small gaps within one pixel or half a pixel were due to the coarse resolution of the AMSR-E image (region A in Fig. 2). Large distances, such as region B in Figure 2, primarily occurred in thin-ice areas with low sea-ice concentration.

Comparison of ASI and MODIS ice concentration ($SIC_{ASI} - SIC_{MODIS}$) at the pseudo-ASPeCt observation points

The correlation of SIC_{ASI} vs SIC_{MODIS} ice concentrations at pseudo-ASPeCt points in each scene is illustrated by the scatter plots in Figure 3. Because all the SIC_{ASI} and SIC_{MODIS} values were collected at sea-ice edges, the points were clustered near the bottom left-hand corner of the plots with low ice concentrations. Many dots have a zero SIC_{ASI} but a non-zero SIC_{MODIS} value, thereby aligning on the left-hand side border of the scatter plot. A large number of these dots will reduce the strength of the correlations, as confirmed by their low R^2 values ($R^2 \leq 0.2$). The test results, however, showed that the correlation coefficients were significantly different from zero, indicating low but significant linear relationships (Table 1).

The bias ($SIC_{ASI} - SIC_{MODIS}$) and RMSE values for each scene are summarized in Table 1. Three of the four scenes had a negative bias, ranging from –15.1% to –12.3%, whereas the fourth scene had a bias close to zero. The average bias for all the sample points was negative, indicating a general underestimation by the AMSR-E ASI products at the sea-ice edges. All the RMSE values were between 19% and 31%, with an average of 27.7%. These values were compared with previous studies, as discussed below.

Comparison of ASI and MODIS ice concentrations ($SIC_{ASI} - SIC_{MODIS}$) along transects

To illustrate the concentration differences in the ice cover along the ice edge, eight transects across the pseudo-ASPeCt observation points were derived from the four scenes (Fig. 4). The order of the starting point, end point and pseudo-ASPeCt point was labeled. All the transects start from the ice interior, pass the ice edges of the pseudo-ASPeCt points and reach 100% open water. Some transects had relatively sharp and compact ice edges (e.g. 2005a), others had more uncertain and gradual edges (e.g. 2009b), and others had obvious low-concentration segments in the interior ice region (e.g. 2004b and 2005b). The R^2 values of a regression between SIC_{ASI} vs SIC_{MODIS} along the transects ranged between 0.69 and 0.96 and were therefore much higher than the values observed at the pseudo-ASPeCt points along the ice edge. Clearly, strong agreement exists between SIC_{ASI} and SIC_{MODIS} in the inner dense ice zones and in the open sea areas, whereas the differences in the transition zones were larger, with generally higher SIC_{MODIS} values.
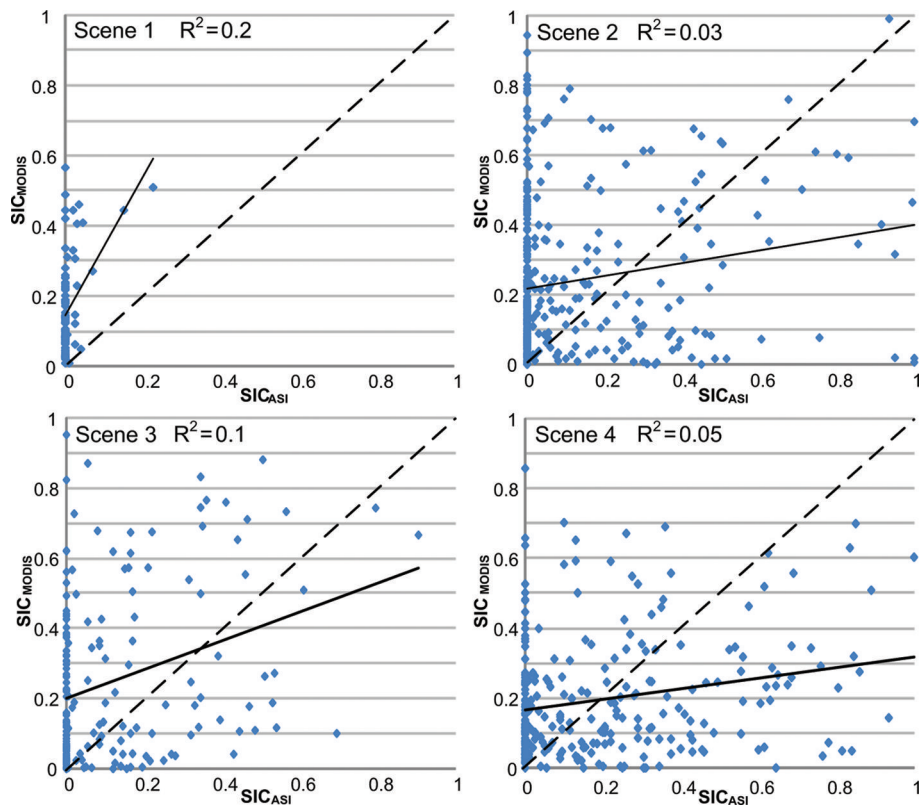
Fig. 3. Sea-ice concentrations from SIC_{ASI} vs SIC_{MODIS} at pseudo-ASPeCt observation points in four scenes. The solid black line represents the best linear fit of the data and the dashed line represents a 1 : 1 relationship.
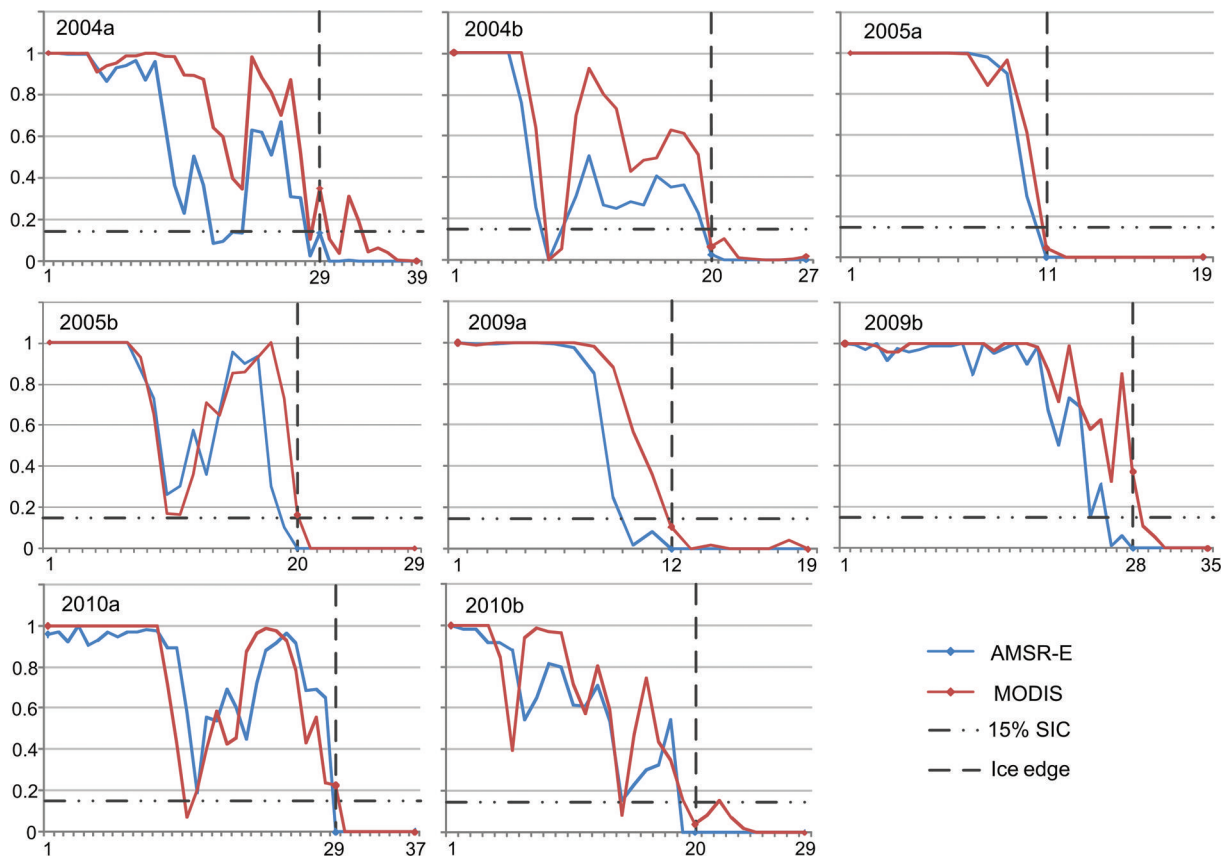

Fig. 4. Sea-ice concentrations from SIC_{ASI} vs SIC_{MODIS} along eight transects. The *x*-axis units are pixels. The vertical dashed lines represent the location of the pseudo-ASPeCt observation points, and the horizontal dotted and dashed lines show the 15% passive microwave concentration.
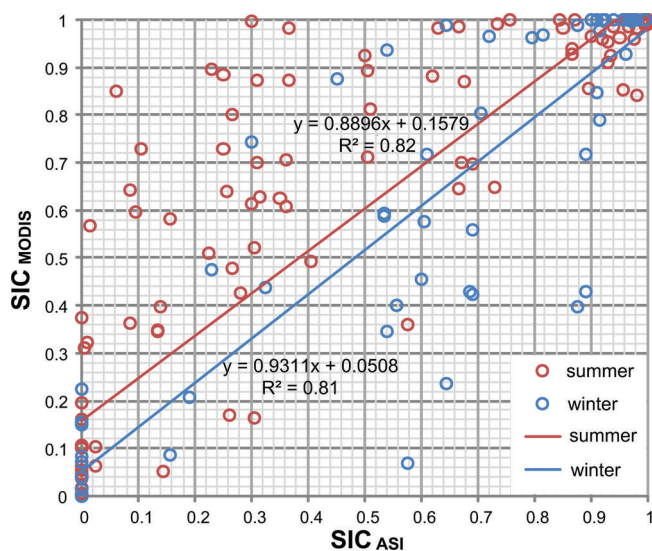
Fig. 5. Scatter plot of SIC$_{ASI}$ vs SIC$_{MODIS}$ from all ASI pixels in eight transects.

This underestimation of SIC$_{ASI}$ in the marginal zone is consistent with our results (Fig. 3).

The vertical dashed lines in Figure 4 represent the locations of the ice edge as observed from the pseudo-ASPeCt points, and the horizontal dotted and dashed lines represent the 15% ice concentration threshold. At the locations of the ice edge, only the SIC$_{ASI}$ in 2004a achieved a 15% threshold, whereas all the others were below 15%. However, the comparisons in Table 1 show a higher mean SIC$_{ASI}$ over 15% in scene 4 in 2010. This inconsistency suggests that the small number of ship-based observations at the ice edge cannot accurately represent the overall ice-edge line. Combining the transect analysis with robust statistics based on a large number of points generated from our proposed method provides a full understanding of the data quality. The distance between a pseudo-ASPeCt point and the northernmost SIC$_{ASI}$ pixel with at least a 15% SIC were all between zero and three pixels wide, with an average of 1.625 pixels (~10 km). These values are in good agreement with our observations (Fig. 2).

Separating the data into summer (scenes 1, 2 and 3) and winter (scene 4) highlights the underestimation of SIC$_{ASI}$ in summer: many more red points lie above the diagonal than below it (Fig. 5). In contrast, the blue points are distributed more evenly around the diagonal and do not have a large bias. The overall R^2 values were 0.82 and 0.81 in summer and winter, respectively. Figure 5 also revealed that the majority of points were clustered in the top right-hand and bottom left-hand corners, i.e. located in the ice interior and in 100% open water, respectively. Only a small portion of the points had moderate ice concentrations and most were scattered far from the regression lines. This suggests that the high correlation coefficient values were mainly attributable to the major corner points, and the small number of ice edge points prohibited further conclusions being drawn from this transect analysis.

DISCUSSIONS

The objective of this study was the localization of sea-ice edges and their corresponding ASI concentration. Previous research (e.g. Worby and Comiso 2004; Ozsoy-Cicek and others, 2011) also compared the 15% threshold from passive microwave images with the ice edges observed from higher-resolution images or from ships, but there was no standard definition of the ice edge when it was extracted from higher-resolution images. Difficulties also occurred when the ship records were sparse at the exact ice-edge locations. Using the ASPeCt ice-edge definition, we retrieved ice concentrations from a MODIS image and determined the ice-edge points using a 2 km resolution in accordance with ASPeCt. This method takes advantage of using easily acquired (MODIS) imagery to generate a large number of pseudo-ASPeCt observations for each scene, and hence contributes to a robust statistical analysis of ice-edge accuracy.

Statistical analysis indicated that the ASPeCt observations, for all scenes and on average, have significantly different mean concentrations from the 15% concentration, although some were close to this value. The correlation between SIC$_{ASI}$ and SIC$_{MODIS}$ values at the ice edge was low ($R^2 \le 0.2$), but all the linear relationships were statistically significant. These correlation coefficients were lower than those reported in previous studies (e.g. Ozsoy-Cicek and others, 2011). This may have resulted from the different ice concentration retrieval methods (ASI vs NT2). However, it is more likely due to the fact that our research relied on a much larger number of samples, which were located exactly at the ice edge instead of within the marginal ice zone. Therefore, simulated pseudo-ship observations and quantitative comparisons in this study helped us to gain a better understanding of the performance of AMSR-E concentration products along the ice edge.

In spite of the significantly different concentration values, the distances between the generated ice edges and the 15% threshold were within three AMSR-E pixels and an average of ~10 km. Many large gaps occur in areas with thin ice and low ice concentrations, which can be explained by the following three phenomena:

1. As thin ice often appears dark with near-freezing temperatures, there is the potential for significant uncertainty when discriminating thin ice from surrounding open water using visible and infrared MODIS image bands (Riggs and others, 2006).

2. When using the 6.25 km resolution channels and output concentration of 6.25 km, the ASI algorithm uses lower-frequency channels with lower spatial resolution for weather filtering, which removes spurious ice concentrations in open water at ice edges (Spreen and others, 2008). The resolution of these weather-filtering channels is ~15–20 km, which is approximately three gridcells.

3. Some of the difference may be a result of a temporal sampling issue. The AMSR-E data are a daily average, whereas the MODIS data are a snapshot. It is possible that the difference in sampling time may reach 24 hours. A substantial amount of sea ice can grow within 24 hours, depending on the conditions. For example, ice missed by the ASI (Fig. 2) may be newly formed ice.

Generally, the 10 km separation is within an acceptable range of accuracy compared with other passive microwave ice concentration products, which have coarser spatial resolutions (e.g. 12.5 and 25.0 km). This finding is similar to a previous conclusion that an average distance of

~12 km exists between the 15% threshold and the SAR-derived edges (Heinrichs and others, 2006). A comparison between the generated pseudo-ice edges and the US National Ice Center (NIC) sea-ice chart should be addressed in a future study.

Our comparison of AMSR-E ASI and MODIS data indicated that the AMSR-E ASI products tend to underestimate the ice concentrations at the ice edges, especially during the Antarctic summer. Another ice concentration algorithm, NT2, applied to AMSR-E images obtained similar results. For example, Heinrichs and others (2006) and Ozsoy-Cicek and others (2009) noted that the AMSR-E NT2 products tended to underestimate low ice concentrations in areas with thin ice, both during the Antarctic summer and the Arctic spring. More specifically, some studies further classified the thin-ice area as new ice, young ice and first-year ice (Cavalieri and others, 2006, 2010), and discovered that a higher fraction of new ice and open water could lead to a larger negative bias of AMSR-E NT2 relative to MODIS or Landsat. Wiebe and others (2009) examined AMSR-E ASI products from Landsat-7 ETM+ and SAR images during the Arctic spring. They reported little underestimation of ASI products for both young ice and first-year ice and larger errors for new ice. For the Antarctic, our results gave a slightly larger negative bias and larger RMSE values at the ice edge derived from an ASI algorithm. In the future, the ice type classification can be applied to our collected Landsat Thematic Mapper (TM) images for detailed error assessment.

The daily average ice concentration product was chosen for this research because it is distributed publicly and is used widely. Therefore, users of the products can benefit from our quality assessment. To track ice-edge movement more precisely, the daytime (ascending pass) and night-time (descending pass) AMSR-E images should be selected to minimize their temporal differences from the reference images. Only four images were included here, but more scenes are needed for future study, especially covering the East Antarctic region. However, the proposed method for generating a large number of ice-edge ASPeCt observations can be applied to the assessment of other passive microwave images and to other ice concentration algorithms.

CONCLUSIONS

This study generated pseudo-ship observations from MODIS images based on the definition of ice-edge points from the ASPeCt protocol. We used these observations to evaluate sea-ice concentrations of AMSR-E ASI at the ice edge. In total, 917 points were sampled from the three MODIS scenes during the Antarctic summer and from one scene in winter. Our statistical tests indicated that the ASI pixels passing pseudo-ASPeCt observations had a mean value of 13% and were significantly different from the 15% threshold. The spatial separation between the pseudo-ice edges and the contour of the 15% threshold was within three 6.25 km pixels and ~10 km on average. Comparing this with the ice concentrations derived from MODIS, we found that the ASI products tended to underestimate the concentration at the ice edge, especially during the summer. Their correlations were surprisingly poor, with R^2 values <0.2. This was due to the large number of zero ASI pixels that could not detect thin ice with low concentrations at the ice edge. From a transect analysis that covered the ice interior, marginal ice zone and open water, we obtained correlation coefficients >0.8. Large differences in ice concentrations existed in the marginal ice zone and ice edge, whereas small differences occurred in the interior and water areas. Underestimation of SIC_{ASI} occurred across the region in the summer and no apparent bias occurred during the winter. This newly developed method provides a way of generating a new source of reference data, in which the spatial coverage is wider and more flexible than for traditional in situ observations. It can also be used in other places, to assess ice concentration products using rigorous statistical analysis.

REFERENCES

Cavalieri DJ, Markus T, Hall DK, Gasiewski AJ, Klein M and Ivanoff A (2006) Assessment of EOS Aqua AMSR-E Arctic sea ice concentrations using Landsat-7 and airborne microwave imagery. *IEEE Trans. Geosci. Remote Sens.*, **44**(11), 3057–3069 (doi: 10.1109/TGRS.2006.878445)

Cavalieri DJ, Markus T, Hall DK, Ivanoff A and Glick E (2010) Assessment of AMSR-E Antarctic winter sea-ice concentrations using Aqua MODIS. *IEEE Trans. Geosci. Remote Sens.*, **48**(9), 3331–3339 (doi: 10.1109/TGRS.2010.2046495)

Heinrichs JF, Cavalieri DJ and Markus T (2006) Assessment of the AMSR-E sea-ice concentration product at the ice edge using RADARSAT-1 and MODIS imagery. *IEEE Trans. Geosci. Remote Sens.*, **44**(11), 3070–3080 (doi: 10.1109/TGRS.2006.880622)

Kaleschke L and 6 others (2001) SSM/I sea ice remote sensing for mesoscale ocean–atmosphere interaction analysis. *Can. J. Remote Sens.*, **27**(5), 526–537

Lee H and Han H (2008) Evaluation of SSM/I and AMSR-E sea ice concentrations in the Antarctic spring using KOMPSAT-1 EOC images. *IEEE Trans. Geosci. Remote Sens.*, **46**(7), 1905–1912 (doi: 10.1109/TGRS.2008.916479)

Markus T and Cavalieri DJ (2000) An enhancement of the NASA Team sea ice algorithm. *IEEE Trans. Geosci. Remote Sens.*, **38**(3), 1387–1398 (doi: 10.1109/36.843033)

Massom RA and Stammerjohn SE (2010) Antarctic sea ice change and variability – physical and ecological implications. *Polar Sci.*, **4**(2), 149–186 (doi: 10.1016/j.polar.2010.05.001)

Ozsoy-Cicek B, Xie H, Ackley SF and Ye K (2009) Antarctic summer sea ice concentration and extent: comparison of ODEN 2006 ship observations, satellite passive microwave and NIC sea ice charts. *Cryosphere*, **3**(1), 1–9 (doi: 10.5194/tc-3-1-2009)

Ozsoy-Cicek B, Ackley SF, Worby A, Xie H and Lieser J (2011) Antarctic sea ice extents and concentrations: comparison of satellite and ship measurements from International Polar Year cruises. *Ann. Glaciol.*, **52**(57 Pt 2), 318–326 (doi: 10.3189/172756411795931877)

Parkinson CL and Cavalieri DJ (2012) Antarctic sea ice variability and trends, 1979–2010. *Cryosphere*, **6**(4), 871–880 (doi: 10.5194/tc-6-871-2012)

Riggs GA, Hall DK and Salomonson VV (2006) *MODIS Sea Ice Products user guide to Collection 5.* NASA Goddard Space Flight Center, Greenbelt, MD. http://modis-snow-ice.gsfc.nasa.gov

Spreen G, Kaleschke L and Heygster G (2008) Sea ice remote sensing using AMSR-E 89-GHz channels. *J. Geophys. Res.*, **113**(C2), C02S03 (doi: 10.1029/2005JC003384)

Wiebe H, Heygster G and Markus T (2009) Comparison of the ASI ice concentration algorithm with Landsat-7 ETM+ and SAR imagery. *IEEE Trans. Geosci. Remote Sens.*, **47**(9), 3008–3015 (doi: 10.1109/TGRS.2009.2026367)

Worby AP and Allison I (1999) A technique for making ship-based observations of Antarctic sea ice thickness and characteristics. Part I: Observational techniques and results. *Antarct. CRC Res. Rep.* 14

Worby AP and Comiso JC (2004) Studies of the Antarctic sea ice edge and ice extent from satellite and ship observations. *Remote Sens. Environ.*, **92**(1), 98–111 (doi: 10.1016/j.rse.2004.05.007)